Nuclear Physics A397 (1983) 343–364

A STUDY OF THE $^{26}Mg(^{12}C, ^{12}B)^{26}Al$ CHARGE-EXCHANGE REACTION

A. ETCHEGOYEN†, D. SINCLAIR, S. LIU†† and M. C. ETCHEGOYEN†

Nuclear Physics Laboratory, Oxford, UK

and

D. K. SCOTT††† and D. L. HENDRIE

Lawrence Berkeley Laboratory, Berkeley, California, USA

Received 7 September 1981
(Revised 16 September 1982)

Abstract: The reaction $^{26}Mg(^{12}C, ^{12}B)^{26}Al(5^+, 3^+)$ has been studied using a beam of 102 MeV of ^{12}C. Shell-model, microscopic direct model and finite-range coupled reaction channel (CRC) calculations including recoil effects, have been performed, for comparison with the experimental data. DWBA calculations were performed for the intermediate states of interest in the $^{11}B + ^{27}Al$ and in the $^{13}C + ^{25}Mg$ channels and these results were also compared with the experimental ones. The dominant reaction mechanism for $^{26}Mg(^{12}C, ^{12}B)^{26}Al(5^+, 3^+)$ appears to be the sequential mode.

E | NUCLEAR REACTIONS $^{26}Mg(^{12}C, ^{12}B)$, $E = 102$ MeV; measured $\sigma(\theta)$; deduced reaction mechanism. Microscopic direct, DWBA, coupled reaction channel models.

1. Introduction

Reactions resulting in charge exchange between heavy ions have been observed for a number of projectiles and targets. Most authors have adopted a model based on direct excitation [1–3]) and some others have also performed a coupled reaction channel (CRC) approach [2,4]). It is an open question which picture most accurately describes the reaction mechanism and this work was performed in order to assess the competition between the two processes.

We report in this paper a study of the $^{26}Mg(^{12}C, ^{12}B)^{26}Al$ reaction using a beam of 102 MeV of ^{12}C. The measured cross sections have been compared with theoretical predictions of the microscopic direct model and the CRC approach. The dominant reaction for $^{26}Mg(^{12}C, ^{12}B)^{26}Al(5^+, 3^+)$ seems to be the sequential mode in which a proton (or neutron) is transferred from ^{12}C (or ^{26}Mg) to ^{26}Mg

† Present address: Comisión Nacional de Energia Atómica, Sede Central, Argentina.
†† On leave from Lanzhou University, China.
††† Present address: Cyclotron Laboratory, Michigan State University.

(or ^{12}C) to form states of ^{27}Al (or ^{25}Mg) and this is followed by neutron (or proton) transfer from ^{27}Al (or ^{13}C) to form $^{26}Al(5^+, 3^+)$ and $^{12}B(g.s.)$.

One-step DWBA analyses for one-particle transfer leading to possible intermediate states of the sequential process have been performed. The aim of these calculations is to test both the optical potential and the form factor parameters and also to estimate the effects of deformations on the one-particle transfer form factors and the potential role of inelastic (CCBA) couplings.

The analyses of one- and two-particle transfer reactions have been calculated in the finite-range formalism, including recoil effects. Although zero-range calculations have been carried out successfully for light ion reactions, the approximation is not appropriate for heavy ions. The computer codes used to calculate the one particle transfer reactions are SATURN[5]) which generates the finite-range form factor (with recoil) and MARS[5]) which is a standard DWBA code. For the CRC calculations a computer code SESIME[6]), developed by Proudfoot and Rae from SATURN-MARS has been used. It is a standard CRC program based on the formalism developed by Udagawa *et al.*[7]). It solves the general coupled equations presented in the above mentioned reference using the form factors generated by SATURN and the distorted waves generated by MARS. The overlap function is calculated by a program developed by the authors.

The computational work performed to evaluate the microscopic finite-range direct model cross section was carried out with a recently developed computer code named BERI[8]). The zero-range approximation was avoided because it is only appropriate with lighter projectiles. To our knowledge, all previous calculations within the framework of this model, have been performed using an expansion in coefficients of fractional parentage (CFP) of the multinucleon transition densities rather than the one-body transition density (OBTD) approach chosen for this work (more details will be given in sect. 5). The OBTD formalism is probably more convenient because only wave functions in the initial and final systems need be calculated to obtain the structure information. On the contrary, the CFP expansion requires wave functions for all the relevant intermediate states[9]). The OBTD were evaluated with the aid of the Oxford shell model code[10]). This code is a standard *m*-scheme program. It projects the *m*-scheme basis onto states of good total angular momentum and isospin before calculating the hamiltonian matrix elements and thus greatly reducing the matrix dimension.

The paper is organized as follows. After the presentation of the data, a summary of the direct model and the analysis of the data within this model are given. Then, the one-step DWBA analysis is performed for the one-particle transfers leading to intermediate states of a possible sequential process and finally, the CRC calculation is presented.

2. Experimental procedure

The experiment was performed using a beam of 102 MeV ^{12}C ions from the Berkeley 88 inch cyclotron. The target was a self-supporting ^{26}Mg foil of thickness 250 $\mu g/cm^2$. Reaction products were momentum analysed in the Berkeley magnetic spectrometer [11]) and identified on the basis of time of flight, magnetic rigidity and dE/dx. Absolute cross sections were computed from the yields using the known target thickness (determined after the experiment by weighing), spectrometer solid angle (0.67 msr) and the measured beam charge. The yield of elastically scattered ions was monitored continuously as a check against target deterioration. The systematic error in the cross sections should be less than 25 %. Fig. 1 shows the ^{11}B, ^{13}C and ^{12}B spectra at 11°; the total FWHM resolution is approximately 200 keV.

3. Qualitative analysis of the results

As mentioned in the introduction, the analysis of the ^{11}B and ^{13}C spectra and the calculation of the relevant one-particle transfer cross sections were carried out for the study of a potential intermediate state of the sequential process. The aim of this work was to assess the relative importance of the one- and two-step processes for this charge exchange reaction.

The ^{11}B and ^{12}C spectra show that the reactions selectively populate the states known to have large single-particle spectroscopic factors. These are the ground state ($d_{\frac{5}{2}}$) and the 0.84 MeV ($s_{\frac{1}{2}}$), the 2.981 MeV ($d_{\frac{3}{2}}$) and the 6.48 MeV ($f_{\frac{7}{2}}$) states in ^{27}Al. The populated states in ^{25}Mg are the ground state ($d_{\frac{5}{2}}$) and the 0.5851 MeV state. There could be two doublets in ^{27}Al formed by the $^{27}Al(\frac{1}{2}^+$, 0.84 MeV) and the $^{27}Al(\frac{3}{2}^+$, 1.014 MeV) states and by the $^{11}B(\frac{1}{2}^-$, 2.12 MeV) and the $^{27}Al(\frac{7}{2}^+$, 2.210 MeV) states. The $(2J_f+1)C^2S$ factors for the two peaks in the first doublet are given in ref. [12]). Their values are 0.81 and 0.32, respectively. DWBA calculations using these factors show that the peak is mainly composed of the $\frac{1}{2}^+$ state. The $\frac{7}{2}^+$ state in the other doublet can be discarded because such a state cannot be populated by a direct process. The ^{13}C spectrum presents a broad peak at approximately 3.5 MeV. The candidates are: the $^{25}Mg(\frac{5}{2}^+$, 3.90 MeV), the $^{13}C(\frac{1}{2}^+$, 3.09 MeV), the $^{13}C(\frac{3}{2}^-$, 3.68 MeV) and the $^{13}C(\frac{5}{2}^+$, 3.85 MeV) states. The spectroscopic factor for the ^{25}Mg candidate is 15 times smaller than that for its ground state and therefore, it can be inferred that the contribution of this excited state is negligible. It can also be added that the experimental data for the $^{25}Mg(^{13}C, ^{14}C)^{25}Mg$ reaction [13]) show that the ^{25}Mg ground state is the only $\frac{5}{2}^+$ state populated with any reasonable strength. Glover *et al.* [14]) extracted spectroscopic factors of 0.9, 0.26 and 0.8 for the $\frac{1}{2}^+$, $\frac{5}{2}^-$ and $\frac{5}{2}^+$ ^{13}C states respectively. Because of the relatively large spectroscopic factor and the high-spin selectivity of this

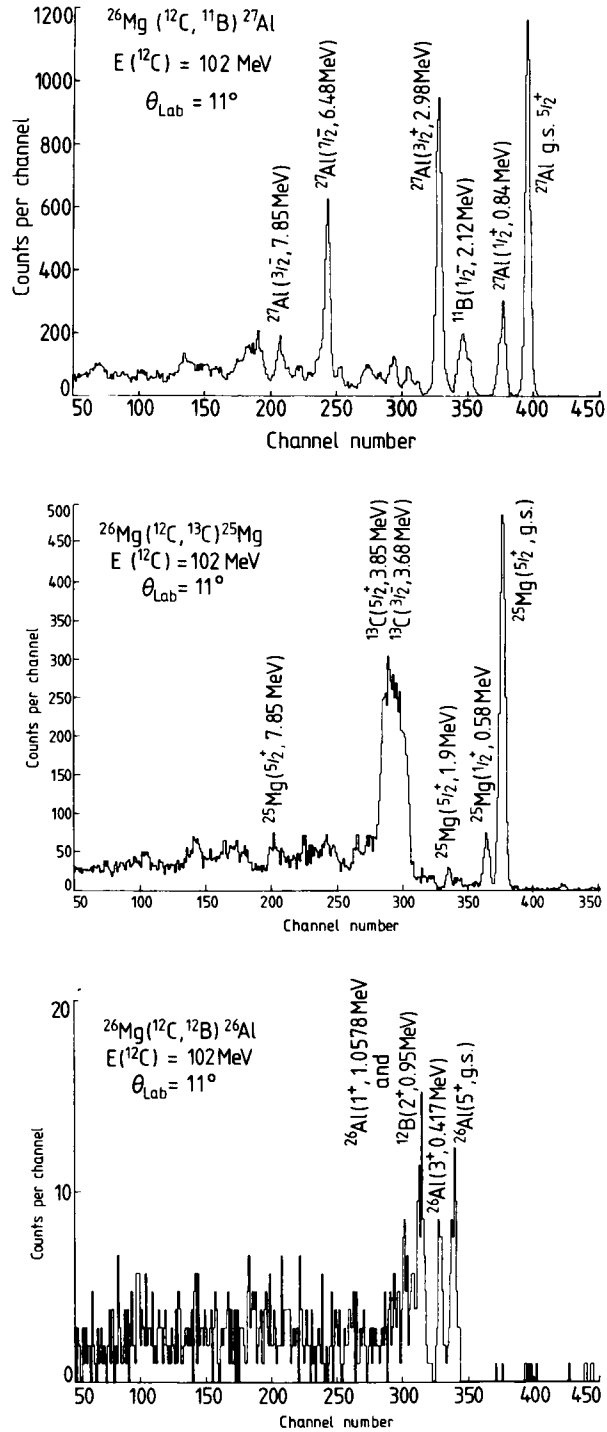

Fig. 1. Experimental spectra for the $^{26}Mg(^{12}C, ^{11}B)^{27}Al$, $^{26}Mg(^{12}C, ^{13}C)^{25}Mg$ and $^{26}Mg(^{12}C, ^{12}B)^{26}Al$ reactions at 11°.

reaction, the $\frac{5}{2}^+$ state is expected to be the predominant contribution to this broad peak in the ^{13}C spectrum.

The ^{25}Mg states at 0.97 MeV and 2.80 MeV are almost unpopulated because of very low spectroscopic amplitudes: 0.06 and 0.17 respectively.

The ^{12}B spectrum presents only three peaks. It is interesting to notice that the $^{26}Al(0^+, 0.23$ MeV) state is not populated to any significant extent. The direct $0^+ \rightarrow 0^+$ transition is forbidden, but the reaction could take place in a sequential manner. Duhm *et al.*[4]) populated this state in the $^{26}Mg(^6Li, ^6He)^{26}Al$ reaction at $E(^6Li) = 32$ MeV and reproduced the angular distribution by a two-step calculation.

A CRC calculation has been performed for this level including four intermediate routes

$$^{26}Mg(0^+) \rightarrow {}^{25}Al(\tfrac{5}{2}^+, \tfrac{1}{2}^+) \rightarrow {}^{26}Al(0^+)$$

and

$$^{26}Mg(0^+) \rightarrow {}^{25}Mg(\tfrac{5}{2}^+, \tfrac{1}{2}^+) \rightarrow {}^{26}Al(0^+),$$

together with the corresponding lighter system routes

$$^{12}C(0^+) \rightarrow {}^{13}C(\tfrac{1}{2}^+) - p_{\frac{1}{2}} \rightarrow {}^{12}B(1^+);$$

that is, the two routes in each mass partition that most strongly contribute to the $^{26}Al(5^+, 3^+)$ cross sections. The parentage amplitudes for $^{26}Al(0^+, T = 1, 0.23$ MeV) are the same as for $^{26}Mg(0^+, T = 1$, g.s.) and they are shown in tables 6 and 7. The cross section obtained is more than two orders of magnitude smaller than the $^{26}Al(5^+, 3^+)$ cross sections, as expected from the analysis of the data.

4. Distorted-wave theory

Following ref. [7]) we write the transition amplitude for a reaction between an incident channel "α" and final channel "β" as

$$T_{\alpha\beta} = T_{\alpha\beta}^{(1)} + T_{\alpha\beta}^{(2)} + T_{\alpha\beta}^{(NO)}. \tag{1}$$

Here, $T_{\alpha\beta}^{(1)}$ is the simultaneous amplitude, $T_{\alpha\beta}^{(2)}$ is the sequential amplitude and $T_{\alpha\beta}^{(NO)}$ is the non-orthogonality correction arising from the selection of the basis state set.

This last contribution depends on the representation used for the interaction matrix elements. If the prior-post form is used (as in this paper), $T_{\alpha\beta}^{(NO)}$ actually vanishes.

5. The one-step contribution

The one-step contribution has been analysed within the framework of the microscopic one-step direct-charge-exchange model. In this model both the projectile and ejectile are given the same spatial coordinates, therefore the $T^{(1)}_{\alpha\beta}$ matrix will be similar in form to the zero-range T-matrix.

Closely following ref. [1,2]) we write, for an A(a, b)B reaction,

$$T^{(1)}_{\alpha\beta} = \int X^{(-)}_{\beta}{}^{*}(\boldsymbol{R}) \langle \mathrm{Bb}|V_{\alpha}|\mathrm{Aa}\rangle X^{(+)}_{\alpha}(\boldsymbol{R}) \mathrm{d}\boldsymbol{R}, \tag{2}$$

where X_{α}, X_{β} are the distorted waves in the incident and exit channels and

$$F(\boldsymbol{R}) = \langle \mathrm{Bb}|V_{\alpha}|\mathrm{Aa}\rangle = \langle I_{\mathrm{B}} T_{\mathrm{B}} s_{\mathrm{b}} t_{\mathrm{b}}|V_{\alpha}|I_{\mathrm{A}} T_{\mathrm{A}} s_{\mathrm{a}} t_{\mathrm{a}}\rangle \tag{3}$$

is the form factor. V_{α} is the microscopic nucleon-nucleon interaction between the target and the projectile. This matrix comprises all the interesting physical features: the selection rules, the nuclear structure (in the corresponding wave functions) and the type of reaction. X_{α} and X_{β} depict only two elastic scattering states.

The projectile-target interaction V_{α} is assumed to be of the form:

$$V_{\alpha} = \sum_{\substack{i\in \mathrm{A} \\ j\in \mathrm{a}}} v_{ij}(|\boldsymbol{r}_{ij}|, \boldsymbol{\sigma}(i), \boldsymbol{\sigma}(j), \boldsymbol{\tau}(i), \boldsymbol{\tau}(j)), \tag{4}$$

with

$$\begin{aligned} v_{ij} &= v_{ij}(|\boldsymbol{r}_{ij}|, \boldsymbol{\sigma}(j), \boldsymbol{\sigma}(i), \boldsymbol{\tau}(j), \boldsymbol{\tau}(i)) \\ &= v(|\boldsymbol{r}_{ij}|)\{V_{00} + V_{01}\boldsymbol{\tau}(j)\cdot\boldsymbol{\tau}(i) + V_{10}\boldsymbol{\sigma}(j)\cdot\boldsymbol{\sigma}(i) + V_{11}(\boldsymbol{\sigma}(j)\cdot\boldsymbol{\sigma}(i))(\boldsymbol{\tau}(j)\cdot\boldsymbol{\tau}(i))\}. \end{aligned} \tag{5}$$

Here, $\boldsymbol{\sigma}$ and $\boldsymbol{\tau}$ are the spin and isospin Pauli operators and $|\boldsymbol{r}_{ij}|$ is the distance between the two interacting nucleons.

The spatial coordinate system is displayed in fig. 2.

Defining the quantum numbers l_1, j (l_2, s) as the angular momentum and the total angular momentum transferred to the intrinsic motion of the target (projectile) system, $\boldsymbol{r}_1(\boldsymbol{r}_2)$ as the coordinate for the interacting nucleon in the target (projectile), and l as the total angular momentum transferred between the initial and final systems, the usual result of the decomposition of the form factor into partial waves as shown in ref. [2]) is:

$$F^{jls}_{m_l}(\boldsymbol{R}) = \sum_{\substack{l_1 l_2 s_0 \\ t_0 n_0}} V_{s_0 t_0} d^{jls; l_1 l_2 s_0 t_0 n_0} f^{jls; l_1 l_2 s_0 t_0}_{m_l}(\boldsymbol{R}), \tag{6}$$

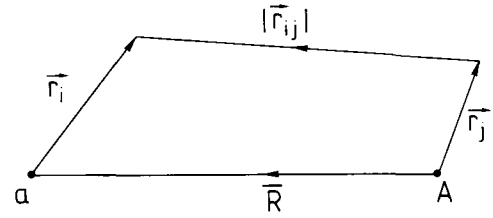

Fig. 2. Coordinate system for the microscopic direct-charge-exchange form factor.

where s_0 and t_0 are either 0 or 1 for the four terms $V_{s_0t_0}$ in equation (5); n_0 is the t_0 projection value, and

$$d^{jl_1s;l_1l_2s_0t_0n_0} = i^{l_2+l-l_1}(-)^{s_a-s_b}\frac{\hat{s}_b}{\hat{s}_a}\,W(jl_1sl_2;s_0l)$$
$$\times(-)^{n_0}\langle T_A N_A t_0 - n_0|T_B N_B\rangle\langle t_a n_a t_0 n_0|t_b n_b\rangle, \tag{7}$$

$$b^{l_1l_2s_0t_0}_{lm_l}(\boldsymbol{R}) = \pi\frac{\hat{l}_1\hat{l}_2}{\hat{l}}\,Y^*_{lm_l}(\hat{\boldsymbol{R}})\sum_{\lambda\lambda'k}\delta_{\lambda+\lambda',l_2}W(l_1\lambda l\lambda';kl_2)\hat{k}\langle l_1\lambda 00|k0\rangle\langle k\lambda' 00|l0\rangle$$
$$\times\int \mathrm{d}r_1\mathrm{d}r_2 r_1^{\lambda+2}r^{\lambda'+2}v_l(r,R)\hat{g}^k_{ab}(r_2)g^{l_1s_0j;t_0}_{AB}(r_1). \tag{8}$$

Here, $g^{l_1s_0j;t_0}_{AB}$ is the heavier system multinucleon transition density:

$$g^{l_1s_0j;t_0}_{AB} = \langle I_B T_B|||\sum_{i\in A}\frac{\delta(r_i-r_1)}{r_i^2}\,\tau^{t_0}(i)T^{l_1s_0j}(i)|||I_A T_A\rangle. \tag{9}$$

The definition for the reduced matrix element is that given by Brink and Sauthier [9]. $\hat{g}^k_{ab}(r_2)$ is the inversion of $g^{l_2s_0s;t_0}_{ab}(r_2)$; $(\boldsymbol{r}_2 = \boldsymbol{r}+\boldsymbol{r}_1)$;

$$\hat{g}^k_{ab}(r,r_1) = \int_{-1}^{1} g^{l_2s_0s;t_0}_{ab}(|\boldsymbol{r}+\boldsymbol{r}_1|)|\boldsymbol{r}+\boldsymbol{r}_1|^{-l_2}P_k(\cos\theta)\mathrm{d}(\cos\theta); \tag{10}$$

and also, $v_l(r,R)$ comes from the inversion

$$v_l(r,R) = \int_{-1}^{1} v(\boldsymbol{r},\boldsymbol{R})P_l(\cos\theta)\mathrm{d}(\cos\theta). \tag{11}$$

The transition density matrices will now be decomposed in one-body transition density matrices in the usual manner.

A one-body operator acting on a system of N-active particles can be expressed as:

$$O_{kg} = \sum_{j=1}^{N} O_{kg}(j), \tag{12}$$

where $O_{kg}(j)$ is the one-body operator acting on particle j. The corresponding form in the second quantization formalism [15]) is:

$$O_{kg} = \sum_{\rho_i \rho_j} (-)^{2k}(2\rho_i+1)^{\frac{1}{2}}\langle \rho_i \| O_k \| \rho_j \rangle \{a^+_{\rho_i} \tilde{a}_{\rho_j}\}^k_g (2k+1)^{-\frac{1}{2}}. \tag{13}$$

The summation runs over all possible single-particle states $\rho_i = |n_i l_i j_i t_i\rangle$.

We now use (13) in the expression of the transition density (9) for the operator $\sum_{i \in A} (\delta(r_i - r_1)/r_i^2)\, \tau^{t_0}(i) T^{l_1 s_0 j}(i)$:

$$g^{l_1 s_0 j; t_0}_{AB}(r_1) = \sum_{\rho_i \rho_j} (2(2j_i+1))^{\frac{1}{2}} \phi_{n_i l_i j_i}(r_1) \phi_{n_j l_j j_j}(r_1) \times \langle l_i j_i \| T^{l_1 s_0 j} \| l_j j_j \rangle \langle t_i \| \tau^{t_0} \| t_j \rangle \langle I_B T_B \| \{a^+_{\rho_i} \tilde{a}_{\rho_j}\}^{j, t_0} \| I_A T_A \rangle (2k+1)^{-\frac{1}{2}}. \tag{14}$$

We shall now consider the special case $s_0 = t_0 = 1$. As it will be shown later, it is the only term in the nucleon-nucleon force that contributes to the present reaction;

$$g^{l_1 1 j; 1}_{AB}(r_1) = \sqrt{6} \sum_{\rho_i \rho_j} (2j_i+1)^{\frac{1}{2}} \langle l_i j_i \| T^{l_1 1 j} \| l_j j_j \rangle \, \mathrm{OBTD}(AB \rho_i \rho_j; j) \times \phi_{n_i l_i j_i}(r_1) \phi_{n_j l_j j_j}(r_1), \tag{15}$$

where the one-body transition density is defined as:

$$\mathrm{OBTD}(AB \rho_i \rho_j; j) = (2k+1)^{-\frac{1}{2}} \langle I_B T_B \| \{a^+_{\rho_i} \tilde{a}_{\rho_j}\}^{j1} \| I_A T_A \rangle. \tag{16}$$

An analytical expression for the $T^{l_1 s_0 j}$ matrix elements can be found in ref. [16]).

Eq. (15) can be written in a more compact way by defming the $C_{\rho_i \rho_j}$ coefficients in the following way:

$$g^{l_1 1 j; 1}_{AB}(r_1) = \sum_{\rho_i \rho_j} c_{\rho_i \rho_j}(l_1 j) \phi_{n_i l_i j_i}(r_1) \phi_{n_j l_j j_j}(r_1). \tag{17}$$

The expression for the lighter system transition density matrix is obviously similar to (17).

Following this formulation, and with the definition of the radial form factor $F^{jls}(R)$ as [1,2])

$$F^{jls}_{m_l}(\boldsymbol{R}) = Y^*_{lm_l}(\hat{\boldsymbol{R}})F^{jls}(R), \tag{18}$$

the final expression for the cross section is that presented in ref. [5]).

6. One-step reaction numerical calculations

6.1. EVALUATION OF THE TRANSITION DENSITIES

In order to perform the one-step reaction numerical calculation, a code named BERI [8]) has been written. This code uses the one-body transition densities produced by the Oxford shell model code [10]) to obtain the $C_{\rho_i\rho_j}$ coefficients defined in eq. (17). It then calculates the radial form factor as defined in (6) and (18) using the bound-state wave functions generated by the code SATURN [5]) and finishes the calculation by coupling to the code MARS [5]).

The link between the Oxford shell model code and the form factor calculation was performed so as to try to have as accurate $C_{\rho_i\rho_j}$ coefficients as possible. It is reasonable to think that the relative phases and magnitudes of these coefficients are as important to the one-step calculation as those of the spectroscopic amplitudes are for the two-step one. Wharton *et al.* [3]) pointed out that the here-called $C_{\rho_i\rho_j}$ coefficients are the main uncertainty in charge-exchange calculations. Kim *et al.* [2]) found that in the $^{28}Si(^{18}O, ^{18}F)^{28}Al$ reaction the magnitude of the $l_2 = 0$ form factor dominates both the 3^+ and the 2^+ cross sections because the single-particle charge-exchange components interfere constructively while in the $l_2 = 2$ form factor they interfere destructively. Gaarde *et al.* [17]) found that the $^{48}Ca(^6Li, ^6He)^{48}Sc(1^+)$ cross section decreases by a factor of 7 due to configuration mixing. This strong dependence was found by just increasing the number of configurations from one to two. The other important aspect to be considered in the one-step model are the radial wave functions that appear in (17). The shape of these wave functions may not alter significantly the shape of the angular distribution provided that the wave functions decay with the binding energy of the bound particle. However, the magnitude of the cross section depends strongly on these functions. As these reactions are surface reactions owing to the short range of the nuclear force and the strongly absorbent feature of the imaginary part of the optical potential, the value of the cross section will be roughly proportional to the square of the transition density at the surface region. As stated and shown for stripping reactions [18]), wave functions that decay with wrong tails, can produce drastic effects in the cross section. In the present paper, the bound-state wave functions have been generated by varying the depth of a Saxon-Woods potential so as to bind the particle at the correct binding energy.

The $C_{\rho_i\rho_j}$ coefficients for the lighter system were obtained by assuming p-shell wave functions. The two-body interaction used was the Cohen and Kurath [19]) one. For the heavier system a Chung and Wildenthal hamiltonian [20]) was assumed and the calculation was restricted to the $d_{\frac{5}{2}}$-$s_{\frac{1}{2}}$ shells. The $d_{\frac{3}{2}}$ shell was not included because such a large calculation can not be performed at present. The effect of the $d_{\frac{3}{2}}$ shell should be small for the ground state and 3^+ state wave functions because it lies very high in energy: the first $\frac{3}{2}^+$ state in ^{17}O lies at 5.08 MeV of excitation energy. Neither does it contribute to the ground-state wave function as an active shell: a spin transfer of 5 with only two particles can only be performed with transfers to or from the $d_{\frac{5}{2}}$ shell.

6.2. EVALUATION OF THE FORM FACTOR

The $^{26}Mg(J = 0^+, T = 1) \rightarrow {}^{26}Al(J = 5^+, 3^+, T = 0)$ has to be produced by a simultaneous "spin and isospin flip". Only the $\sigma \cdot \sigma\tau \cdot \tau$ term in the nucleon-nucleon force can accomplish this: the conservation of the heavier system parity allows only an even angular momentum transfer to the intrinsic motion, l_1, and m order to populate an odd total angular momentum in the residual nucleus, the intrinsic spin transfer should be one. It is also immediately seen that the selection rule $\Delta(T_A, T_B, T)$ can only hold when $T = 1$.

Three different nucleon-nucleon forces were used:

a Yukawa type,

$$v(|r_{ij}|) = V_{11} \exp\left[-\left(\frac{|r_{ij}|}{\beta_1}\right)\Big/\left(\frac{|r_{ij}|}{\beta_1}\right)\right];$$

a gaussian type,

$$v(|r_{ij}|) = V_{11} \exp\left[-\left(\frac{|r_{ij}|^2}{\beta_2^2}\right)\right];$$

and the effective nucleon-nucleon interaction introduced by Bertsch *et al.* [21])

$$v(r_{ij}) = -2105.1 \frac{\exp[-4|r_{ij}|]}{4|r_{ij}|} + 653.6 \frac{\exp[-2.5|r_{ij}|]}{2.5|r_{ij}|} + 1.3 \frac{\exp[-0.707|r_{ij}|]}{0.707|r_{ij}|}.$$

In the present calculation β_1 was set to 1.0 fm and β_2 to 1.8 fm.

For the Yukawa and gaussian interactions the strength of the force V_{11}, was the only free parameter to be fixed so as to normalize the computed cross section to the experimental one,

$$\left(\frac{d\sigma}{d\Omega}\right)_{exp} = V_{11}^2 \left(\frac{d\sigma}{d\Omega}\right)_{computed},$$

whereas, the Bertsch interaction has no free parameters.

TABLE 1

Optical potentials for $^{26}Mg + ^{11}B$, $E(^{11}B) = 114$ MeV

	V_R	r_{0R}	$a_R = a_s$	W_V	$r_{0V} = r_{0s}$	a_V	W_s	$\frac{\sigma_{th}(A_i)}{\sigma_{th}(A_1)}$
A1	57	1.072	0.65	25	1.15	0.8	0	1.0
A2	35	1.066	0.80	25	1.22	0.62	0	1.1
A3	106	1.10	0.49	13	1.20	1.0	0	0.75
A4	150	0.946	0.65	70	1.15	0.2	9	1.1

The radial wave functions were generated from a Saxon-Woods potential with geometric parameters $r_0 = r_c = 1.25$ fm, $a_0 = a_{s.o.} = 0.65$ fm and $V_{s.o.} = 7$ MeV. The depth of the potential was obtained from the experimental binding energies on ^{25}Mg and on ^{11}B.

The optical potential used was extracted from ref. [13]). This potential was obtained by fitting the elastic scattering data of ^{11}B colliding on ^{26}Mg at 104 MeV. The parameters are listed as set Al in table 1.

6.2. THE $^{26}Mg(^{12}C, ^{12}B)^{26}Al(5^+)$ REACTION

The obtained $C_{\rho_i\rho_j}$ coefficients for this reaction are listed in table 2. The three two-body interactions gave similar shapes for both the radial form factor and the cross section. These two results, for the gaussian interactions are displayed in figs. 3

TABLE 2

Lighter system $C_{\rho_i\rho_j}$ coefficients

Final state		Initial state		Transference			OBTD	$T^{l_{2<}1s}$	$T^{l_{2>}1s}$	$C_{\rho_i\rho_j}(l_{2<})$	$C_{\rho_i\rho_j}(l_{2>})$
L	$2J$	L	$2J$	$2s$	$l_{2<}$	$l_{2>}$					
1	1	1	1	2	0	2	0.0194	0.1629	−0.4607	0.0109	−0.0309
1	3	1	3	2	0	2	0.2301	−0.4607	−0.1629	−0.3671	−0.1298
3	3	1	1	2	0	2	0.1131	0.3257	0.1152	0.1805	0.0638
3	3	1	3	2	0	2	0.0255	−0.3642	0.1030	−0.0454	0.0128

Heavier system $C_{\rho_i\rho_j}$ coefficients

(i) $^{26}Mg(^{12}C, ^{12}B)^{26}Al(5^+)$ state

Final state		Initial state		Transference		OBTD	$T^{l_1 1j}$	$C_{\rho_i\rho_j}$
L	$2I$	L	$2J$	$2j$	l_1			
2	5	2	5	10	4	−0.1662	0.6456	−0.6440

TABLE 2 (continued)

(ii) $^{26}Mg(^{12}C, ^{12}B)^{26}Al(3^+)$ state

Final state		Initial state		Transference			OBTD	$T^{l_1<1j}$	$T^{l_1>1j}$	$C_{\rho_i\rho_j}(l_{1<})$	$C_{\rho_i\rho_j}(l_{1>})$
L	$2J$	L	$2J$	$2j$	$l_{1<}$	$l_{1>}$					
2	5	2	5	6	2	4	−0.1407	0.4046	−0.0779	−0.3415	0.0657
2	5	0	1	6	2	4	0.0463	0.4309	0.0000	0.1196	0.0000
0	1	2	5	6	2	4	0.0839	−0.7464	0.0000	−0.2169	0.0000

and 4, respectively. It can be seen that the shape of the cross section is reproduced by the calculation. The form factor is seen to be peaked inside the surface region, partly because the bound-state wave functions are so. This result has already been observed in $^{48}Ti(^3He, ^3H)$ data [22]). In the present reaction the form factor is peaked at 5.3 fm whereas the channel radius at grazing contact is 6.5 fm. At this latter distance the form factor has already diminished by more than 30 % and the final cross section would therefore be 70 % lower in magnitude than it would have been, had it been surface peaked. At the experimental measured angles, no significant difference in the cross sections was found when a lower cut-off of 6.5 fm was made. At more backward angles, for which the projectile and the target have to collide at closer distances, the two cross sections were significantly different, both in magnitude and in shape.

6.4. THE $^{26}Mg(^{12}C, ^{12}B)^{26}Al(3^+)$ REACTION

The $C_{\rho_i\rho_j}$ coefficients for this reaction are listed in table 2.

Figs. 5 and 6 display the gaussian form factor and the cross section for the 3^+ excited state. Again, no difference in shape was encountered among the three different interactions used. The calculation shows again (fig. 5) a clear selectivity for the lower l-transfer value. This is inspite of the kinematic selectivity for high l-transfers and thus reflects the strong l-dependence of the form factors. These two opposing (kinematic and structure) selectivities are partly responsible for the low cross sections.

The values obtained for V_{11} and the normalization for the effective interaction are listed in table 3 and are compared to those obtained elsewhere.

Two other contributions could be taken into account as relevant to the one-step mode: one arising from the nucleon-nucleon tensor force and one arising from exchange effects.

The tensor force is known not to contribute significantly to the cross section [23]). In their study about this force Gaarde *et al.* [24]) found that it makes no contribution to transitions to natural-parity states but affects transitions to unnatural-

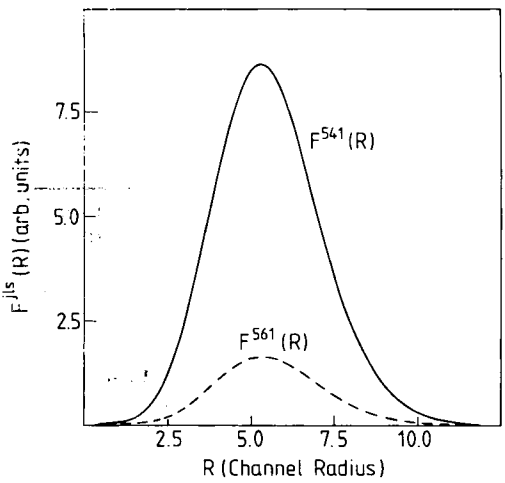

Fig. 3. Radial form factors $F^{jls}(R)$ for a gaussian interaction of range $\beta_2 = 1.8$ fm for the $^{26}Mg(^{12}C, ^{12}B)^{26}Al(5^+)$ reaction.

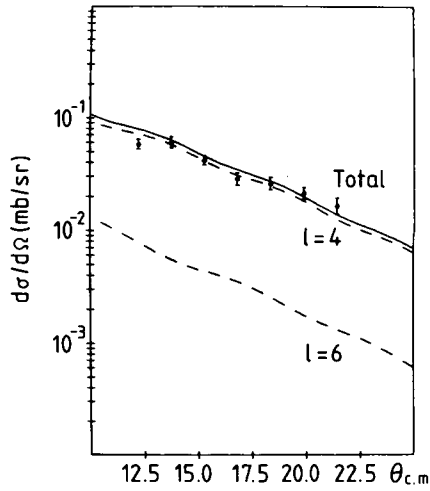

Fig. 4. $^{26}Mg(^{12}C, ^{12}B)^{26}Al(5^+)$ microscopic direct-charge-exchange cross section and partial cross sections for angular momentum transfers of 4 and 6. A gaussian two-body interaction of range parameter $\beta_2 = 1.8$ fm has been used.

parity high-spin states. Even so, this contribution is small: for the 5^+ state in the $^{48}Ca(^6Li, ^6He)^{48}Sc$ reaction, the V_{11} value decreases 11 % when the tensor force is included.

On the other hand, exchange effects may play an important role[25,26]. They could decrease the Yukawa V_{11} strength by a factor of two. Even this factor would not be enough to bring the theoretical value close to the experimental one [(p, p') and (p, n) reactions give, for a 1 fm Yukawa interaction, $V_{11} = 12 \pm 2.5$ MeV, ref. [27])].

The physical interpretation of the unrealistically high V_{11} value is straightforward: the reaction does not proceed through a direct one-step charge-exchange process. As it will be shown later, the above conclusion is reinforced by the magnitude of the sequential cross section, which seems to be the dominant contribution.

7. The two-step contribution

7.1. GENERALITIES

The coupled reaction channel formalism has been described in some detail by many authors[7,28-30]) and only the conclusions will be outlined here.

The second-order T-matrix is found to be composed of the sum of two terms: the sequential and the non-orthogonality terms.

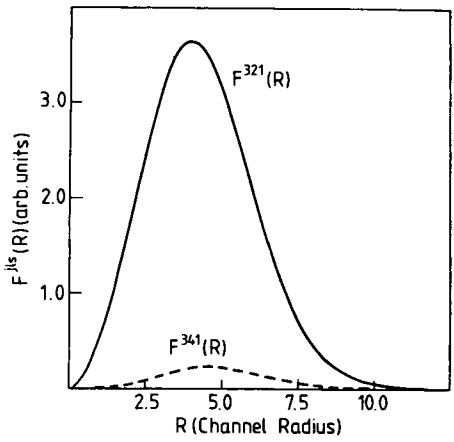

Fig. 5. Radial form factors $F^{jls}(R)$ for a gaussian interaction of range $\beta_2 = 1.8$ fm for the $^{26}Mg(^{12}C, ^{12}B)^{26}Al(3^+)$ reaction.

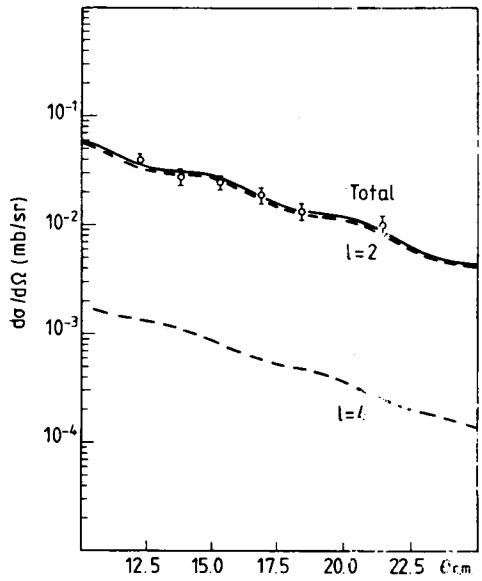

Fig. 6. $^{26}Mg(^{12}C, ^{12}B)^{26}Al(3^+)$ microscopic direct charge-exchange cross section and partial cross sections for angular momentum transfers of 2 and 4. A gaussian two-body interaction of range parameter $\beta_2 = 1.8$ fm has been used.

The physical meaning of the sequential term in charge-exchange reactions is the passage of a nucleon from the projectile to the target (stripping) and then, one from the target to the projectile (pick-up). The reaction also evolves in the opposite

TABLE 3

V_{11} strength (MeV)

Interaction type	(p, n) ref. [34])	(^{6}Li, ^{6}He) ref. [3])	(^{7}Li, ^{7}Be) ref. [35])	$^{28}Si(^{18}O, ^{18}F)$ ref. [2])	$^{26}Mg(^{12}C, ^{12}B)^{26}Al$ (present work)	
					ground state	excited state
gaussian $\beta_2 = 1.8$	7–21			25	38	55
Yukawa $\beta = 1.0$		20–300	15	76	118	167
Bertsch [a])			2–6 [b])	5.3	6.2	10.0

[a]) Bertsch interaction has the force strength already included and the numbers quoted here are those needed to multiply the theoretical force so as to bring the theoretical cross section to agree with the experimental one.

[b]) Single-nucleon knockout exchange effects were added.

direction viz., first pick-up and then stripping. All the important routes should be taken into account and coherently summed.

The other term, the non-orthogonality term has no physical meaning. It arises from the selection, as a matter of convenience, of a non-orthogonal basis: the total wave function describing the system is expanded in terms of different mass partitions (initial, final and intermediate channels). The reason for this is that, expressed as such, it is easily truncated by choosing only those few states of interest.

7.2. DWBA CALCULATIONS

Before going into details of the two-step process, the DWBA calculations for the important intermediate routes will be presented. It is important to have a good fit to the one-step processes through which the different intermediate routes proceed, in order to have confidence in the two-step result.

The influence of the optical potentials was studied and it was concluded that they do not alter the final results significantly. Four different sets extracted from ref. [13]) were tested. No real dependence in neither the shape nor the magnitude of the cross section was found. These test runs were performed for the most important route leading to $^{26}Al(5^+)$: that one through the ground states of ^{11}B and ^{27}Al. The calculations are summarized in table 1. Set Al was used for all the routes, for all the channels and for all the intermediate states.

The cross sections are displayed in figs. 7 and 8. The general fit to the cross sections, both in shape and in magnitude, is good. The fit to the $^{27}Al(\frac{1}{2})^+$ excited state can be seen to be out of phase. This is a long-standing problem, the so-called $l = 1$ anomaly. As seen in dashed lines the difference in phase is removed by increasing the radius of the imaginary part of the exit channel optical potential by 25 %. On the other hand the new normalization (1.7) is worse.

To finish the discussion on the one-particle transfer reactions some assessments will be drawn on possible couplings to inelastic channels. Some reasons suggest that inelastic couplings are not important. (a) All the normalization factors are very close (or even equal) to one showing that DWBA accounts for the magnitude of the cross section. (b) Table 4 shows a comparison of spectroscopic factors obtained in this work and elsewhere and they are in good general agreement. (c) The obvious candidate for an inelastic coupling is $^{12}C(2^+, 4.4391$ MeV). Nevertheless, $^{11}B(\frac{3}{2}^-, 0.0$ MeV) has a spectroscopic factor more than 5 times smaller with $^{12}C(2^+, 4.4391$ MeV) than with $^{12}C(0^+, 0.0$ MeV) and so a two-step process through the 2^+ state would unlikely compete with the one-step process (as will be shown later the intermediate route through (^{11}B $\frac{3}{2}^-$, 0.0 MeV is the most important for both states, 5^+ and 3^+, in ^{26}Al). It is emphasized that higher-order processes (i.e., a sequential transfer plus an inelastic excitation or inelastic excitation plus one-step charge exchange) can not be calculated because no computing codes are available at present and that the great effort involved may not be rewarding.

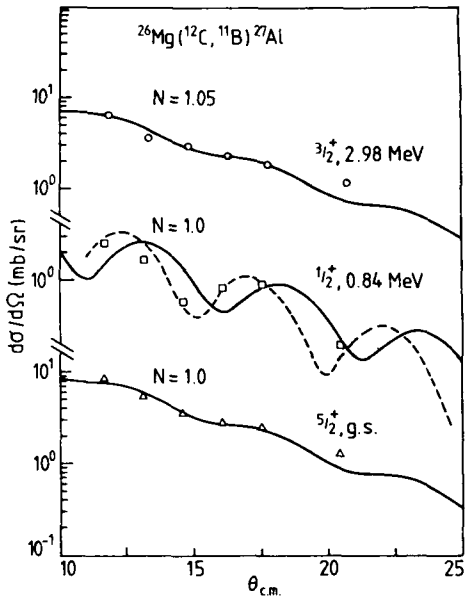

Fig. 7. DWBA fits to the $^{26}Mg(^{12}C, ^{11}B)^{27}Al$ reactions. N is the normalization factor required in order to bring the theoretical cross section to the value of the experimental cross section.

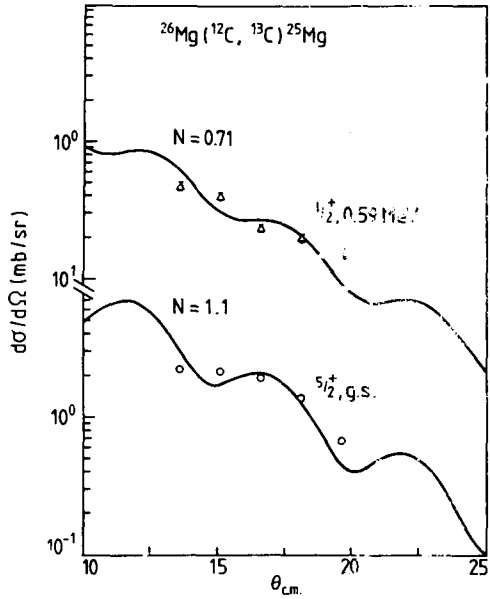

Fig. 8. Differential cross sections for the $^{26}Mg(^{12}C, ^{13}C)$ reaction leading to states in ^{25}Mg.

7.3. COUPLED REACTION CHANNEL CALCULATIONS

Not many calculations have been performed hitherto in the coupled reaction channel scheme, due to the work involved in them. The number of routes through which the reaction can take place, could be prohibitively large even when a highly

TABLE 4

Spectroscopic factors for single-nucleon transfer reactions induced by different projectiles on ^{26}Mg

Residual nucleus	E_x (MeV)	J^π	C^2S heavy ion exp	C^2S light ion exp	C^2S present exp
^{27}Al	0.0	$\frac{5}{2}^+$	0.35 [a])	0.25 [b])	0.36
^{27}Al	0.84	$\frac{1}{2}^+$	0.46 [a])	0.50 [b])	0.46
^{27}Al	2.98	$\frac{3}{2}^+$	0.50 [d])	0.625 [b])	0.57
^{25}Mg	0.0	$\frac{5}{2}^+$	2.00 [a])	2.50 [c])	2.46
^{25}Mg	0.59	$\frac{1}{2}^+$	0.13 [d])	0.17 [c])	0.155

[a]) I. Paschopoulos, P. S. Fisher, N. A. Jelley, S. Kahana, A. A. Pilt, W. D. M. Rae and D. Sinclair, Nucl. Phys. **A252** (1975) 173, ^{11}B beam.

[b]) H. F. Lutz, D. W. Heikkinen, W. Bartolini and T. H. Curtis, Phys. Rev. C2 (1970) 981, ^3He beam.

[c]) D. Dehnhard and J. L. Yntema, Phys. Rev. **160** (1967) 964, d-beam.

[d]) D. Sinclair, I. Paschopoulos, H. S. Bradlow, P. S. Fisher, A. A. Pilt and W. D. M. Rae, Nucl. Phys. **A261** (1976) 511.

truncated basis is chosen. In these cases some important intermediate routes, i.e. some important single-particle configurations in the intermediate system wave functions, have to be omitted. The penalty for this is that very large normalization factors, N, $(d\sigma/d\Omega)_{exp} = N(d\sigma/d\Omega)_{theor}$ have to be introduced *ad hoc* in order to fit the data. In the present calculations all important routes are included and there should be no need for large renormalization factors.

7.4. THE $^{26}Mg(^{12}C, ^{12}B)^{26}Al(5^+)$ REACTION

The above considerations led us to study the $^{26}Mg(^{12}C, ^{12}B)^{26}Al(5^+)$ reaction. Its final spin, 5, can only be reached through the $\frac{5}{2}^+$ states in the intermediate ^{25}Mg and ^{27}Al nuclei. Sum rules show that the ground state in ^{25}Mg carries 74 % of the single-particle strength and in ^{27}Al it carries 77 % (table 5). The one nucleon transfer data (fig. 1) confirms this.

In the lighter system, the $\frac{1}{2}^-$ and $\frac{3}{2}^-$ states should be included for both the ^{13}C and the ^{11}B nuclei. Again, sum rules (table 5) and fig. 1, indicate that only the first one of each spin need be included. The important intermediate routes for the present reaction are summarised in fig. 9.

All the nucleon-transfer reactions were performed using the code SESIME [6]), in the prior-post representation. SESIME was developed from the DWBA code SATURN-MARS [5]).

The heavier system spectroscopic amplitudes, listed in table 6, were obtained with the Oak-Ridge shell model code [31]), using the same hamiltonian as mentioned in the one-step exchange analysis but with a complete sd-shell. The definition used for the spectroscopic amplitudes is that given by Anyas-Weiss *et al.* [32]). The generalized Talmi-Moshinsky bracket is not included in this table.

Fig. 10 displays the final CRC cross section and the experimental one. The different intermediate contributions are also plotted. In the second step of the reaction, the lighter system can either exchange a $p_{\frac{1}{2}}$ or $p_{\frac{3}{2}}$ nucleon, in any route. The separate results for these two modes are independently displayed because the

TABLE 5

	$\frac{C^2S}{G_n^{pu}(T_>)}$	$\frac{2J_f+1}{2J_i+1}\frac{C^2S}{G_p^{st}(T_<)}$	$\frac{C^2S}{G_p^{pu}(T_>)}$	$\frac{2J_f+1}{2J_i+1}\frac{C^2S}{G_n^{st}(T_<)}$
$^{26}Mg \rightarrow {}^{25}Mg(\frac{5}{2}^+)$	0.74			
$^{26}Mg \rightarrow {}^{27}Al(\frac{5}{2}^+)$		0.77		
$^{12}C \rightarrow {}^{11}B(\frac{1}{2}^-)$			0.99	
$^{12}C \rightarrow {}^{11}B(\frac{3}{2}^-)$			0.88	
$^{12}C \rightarrow {}^{13}C(\frac{3}{2}^-)$				0.98
$^{12}C \rightarrow {}^{13}C(\frac{1}{2}^-)$				0.98

The meaning of the indexes in the strength function G is: pu(st), pick-up (stripping) reaction; p(n), proton (neutron) transfer reaction; $T_>$ ($T_<$), final isospin is equal to $T_{initial}+\frac{1}{2}$ ($T_{initial}-\frac{1}{2}$).

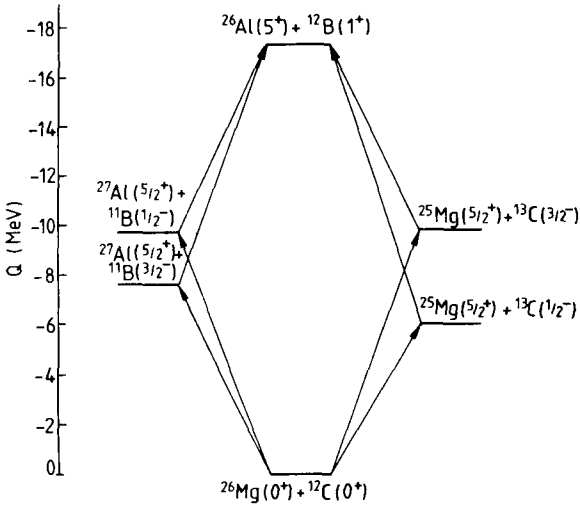

Fig. 9. Intermediate routes considered in the $^{26}Mg(^{12}C, ^{12}B)^{26}Al(5^+)$ CRC calculation.

spectroscopic amplitudes differ for the $p_{\frac{1}{2}}$ and $p_{\frac{3}{2}}$ transfers. The $p_{\frac{1}{2}}$ transfers for both the $^{11}B(\frac{3}{2}^+)$-$^{12}B(1^+)$ reaction and for the $^{13}C(\frac{1}{2}^+)$-$^{12}B(1^+)$ one are not presented since previous calculations showed that they do not alter the final cross section. It can be noticed that the total cross section is larger than the incoherent sum of the several intermediate channels, showing that, for this reaction and in the prior-post representation, the amplitudes interfere constructively.

The shape of the final differential cross section is similar to that obtained in the one-step process and both are in accordance with the experimental one.

The normalization factor N was found to be 2.65.

TABLE 6

Spectroscopic amplitudes used for the $^{26}Mg(^{12}C, ^{12}B)^{26}Al(5^+)$ reaction

	^{27}Al $\frac{5}{2}^+$, 0.0 MeV	^{25}Mg $\frac{5}{2}^+$, 0.0 MeV	^{26}Al 5^+, 0.0 MeV	^{11}B $\frac{3}{2}^-$, 0.0 MeV	^{13}C $\frac{1}{2}^-$, 0.0 MeV	^{11}B $\frac{1}{2}^-$, 2.12 MeV	^{13}C [illegible]	$^{12}B(1^+$ [illegible] MeV)	
								$p_{1/2}$	$p_{3/2}$
$^{26}Mg: 0^+$, 0.0 MeV	−0.68	1.65							
$^{27}Al: \frac{5}{2}^+$, 0.0 MeV			1.09						
$^{25}Mg: \frac{5}{2}^+$, 0.0 MeV			1.07						
$^{12}C: 0^+$, 0.0 MeV				2.39	0.78	1.23	[illegible]		
$^{13}C: \frac{1}{2}^-$, 0.0 MeV									1.34
$^{11}B: \frac{3}{2}^-$, 0.0 MeV								0.4	0.54
$^{13}C: \frac{3}{2}^-$, 3.68 MeV								−0.27	0.22
$^{11}B: \frac{1}{2}^-$, 2.12 MeV									−0.74

We have the heavy system spectroscopic factors by courtesy of B. A. Brown and [illegible] Wildenthal. The phases were obtained with the Oxford Shell Model Code.

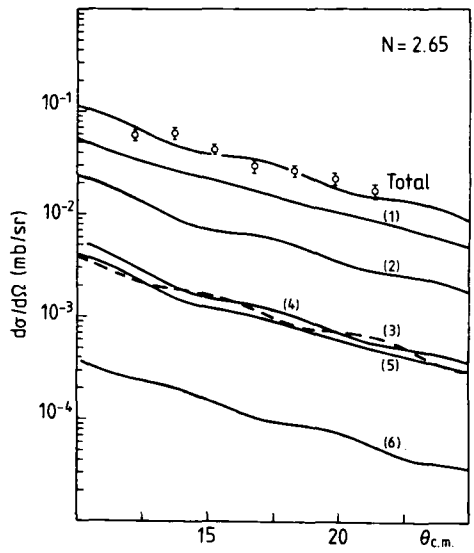

Fig. 10. CRC fit to the experimental $^{26}Mg(^{12}C, ^{12}B)^{26}Al(5^+)$ cross section. The contribution of the calculated intermediate routes are labelled as follows:

(1) $^{11}B(\frac{3}{2}^-)p_{1/2}$, (2) $^{13}C(\frac{1}{2}^-)p_{3/2}$, (3) $^{11}B(\frac{3}{2}^-)p_{3/2}$,
(4) $^{13}C(\frac{3}{2}^-)p_{1/2}$, (5) $^{11}B(\frac{1}{2}^-)p_{3/2}$, (6) $^{13}C(\frac{3}{2}^-)p_{3/2}$,

where, for example: $^{11}B(\frac{3}{2}^-)\,1p_{1/2}$ labels the intermediate route through $^{11}B(\frac{3}{2}^-)$, evolving to ^{12}B by a $1p_{1/2}$ particle transfer.

7.5. THE $^{26}Mg(^{12}C, ^{12}B)^{26}Al(3^+)$ REACTION

Many more intermediate routes are necessary for this state. The complete sd-shell is now an active one.

Fig. 11 shows the intermediate routes considered in this work and fig. 12 displays the cross section. The spectroscopic amplitudes listed in table 7 were obtained with the Oak-Ridge code [31]), unless otherwise stated.

The normalization factor was found to be 2.85.

Tamura *et al.* mention in their review article [33]) that the CRC theory often underestimates the magnitude of the cross section by one or two and sometimes even three orders of magnitude. The present normalization factors are near to one probably because no severe truncation was done on the number of intermediate routes.

8. Conclusion

In this paper we have presented data on the $^{26}Mg(^{12}C, ^{11}B)^{27}Al$,

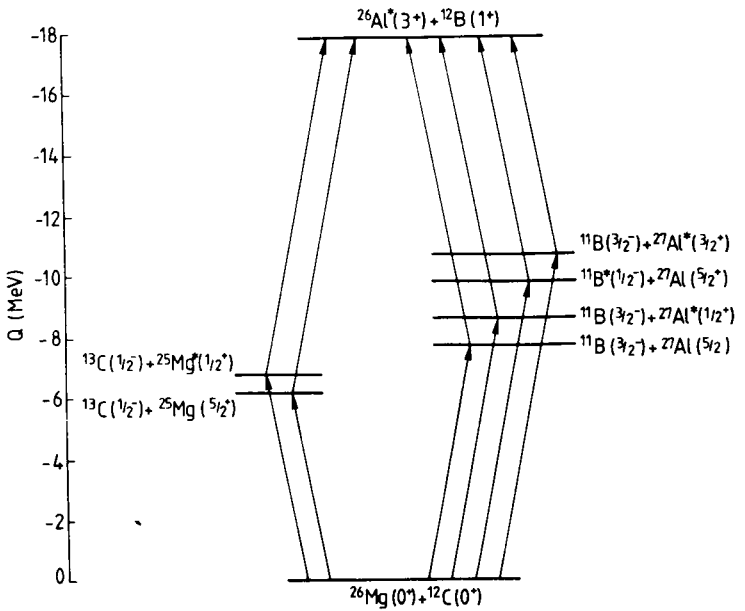

Fig 11. Intermediate routes considered in the $^{26}Mg(^{12}C, ^{12}B)^{26}Al(3^+)$ CRC calculation.

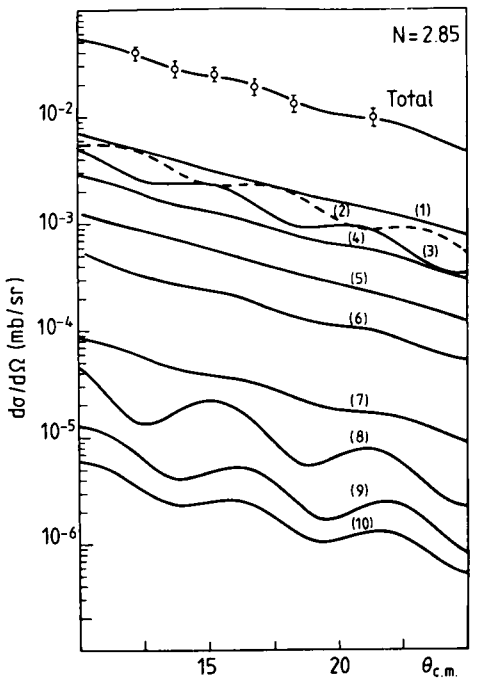

Fig. 12. A CRC fit to the measured $^{26}Mg(^{12}C, ^{12}B)^{26}Al(3^+)$ cross section. The contribution of the various intermediate routes are labelled as follows:

(1) $^{11}B(\frac{3}{2}^-)s_{5/2}p_{1/2}s_{1/2}$ (2) $^{11}B(\frac{3}{2}^-)s_{1/2}p_{1/2}d_{5/2}$
(3) $^{13}C(\frac{1}{2}^-)d_{5/2}p_{3/2}s_{1/2}$ (4) $^{11}B(\frac{3}{2}^-)d_{3/2}p_{1/2}s_{1/2}$
(5) $^{13}C(\frac{1}{2}^-)s_{1/2}p_{3/2}d_{5/2}$ (6) $^{13}C(\frac{1}{2}^-)d_{3/2}p_{3/2}d_{5/2}$
(7) $^{11}B(\frac{3}{2}^-)d_{3/2}p_{1/2}d_{5/2}$ (8) $^{11}B(\frac{3}{2}^-)d_{3/2}p_{1/2}d_{5/2}$
(9) $^{11}B(\frac{3}{2}^-)d_{5/2}p_{3/2}d_{5/2}$ (10) $^{11}B(\frac{3}{2}^-)d_{5/2}p_{3/2}d_{5/2}$

TABLE 7

Spectroscopic amplitudes for the $^{26}Mg(^{12}C, ^{12}B)^{26}Al(3^+)$ reaction

	^{27}Al $\frac{1}{2}^+$ 0.84 MeV	^{27}Al $\frac{3}{2}^+$ 2.98 MeV	^{25}Mg $\frac{1}{2}^+$ 0.59 MeV	^{26}Al 3^+ 0.42 MeV
$^{26}Mg(0^+$, 0.0 MeV)	−0.76	−0.834 [a])	0.347 [a])	
$^{27}Al(\frac{5}{2}^+$, 0.0 MeV)				
$d_{5/2}$				0.10
$s_{1/2}$				−0.387
$^{25}Mg(\frac{5}{2}^+$, 0.0 MeV)				
$d_{5/2}$				0.23
$s_{1/2}$				−0.74
$^{27}Al(\frac{1}{2}^+$, 0.84 MeV)				−0.96
$^{27}Al(\frac{3}{2}^+$, 2.98 MeV)				
$d_{5/2}$				0.69
$d_{3/2}$				−0.18
$^{25}Mg(\frac{1}{2}^+$, 0.59 MeV)				−0.46

[a]) Values taken from D. Sinclair *et al.*, Nucl. Phys. **A261** (1976) 522. See footnote under table 6.

$^{26}Mg(^{12}C, ^{13}C)^{25}Mg$ and $^{26}Mg(^{12}C, ^{12}B)^{26}Al$ reactions at incident ^{12}C energy of 102 MeV. The aim of this work was to decide on the reaction mechanism of the charge exchange reaction leading to the 5^+ and 3^+ state in ^{26}Al. The one-step process was analysed in terms of the microscopic direct charge exchange model and the two-step process in terms of the finite range CRC model. The corresponding cross sections were found to be similar in shape, leaving the absolute magnitudes as the sole way to decide on the mechanism. The one-step process was found not to contribute significantly whereas the sequential mode cross-section magnitude was found to be much larger and close to the experimental value. The dominant reaction mechanism appears to be the sequential mode.

References

1) F. Petrovich and D. Stanley, Nucl. Phys. **A275** (1977) 487
2) B. T. Kim, A. Greiner, M. A. G. Fernandez, N. Lisbona, K. W. Low and M. C. Mermaz, Phys. Rev. C20 (1979) 1396
3) W. R. Wharton and P. T. Wharton and P. T. Deberec, Phys. Rev. C11 (1975) 1963
4) H. H. Duhm, H. Hafner, R. Renfordt, M. Godschmidt, O. Dragun and K-I. Kubo, Phys. Lett. **48B** (1974) 1
5) T. Tamura and K. S. Low, Comp. Phys. Comm. **8** (1974) 349
6) G. Poudfoot and W. D. M. Rae, computer code SESIME (1978), unpublished
7) T. Udagawa, H. H. Wolter and W. R. Coker, Phys. Rev. Lett. **31** (1973) 1507
8) A. Etchegoyen, BERI (1980), unpublished
9) D. M. Brink and G. R. Satchler, Angular momentum, Oxford Library of the Physical Sciences (1975)
10) N. S. Godwin and W. D. M. Rae, Oxford shell model code (1979), unpublished
11) D. L. Hendrie, Nuclear spectroscopy and reactions, ed., J. Cerny part A (1974) p. 365
12) J. Uzureau, A. Adam and S. Joly, Nucl. Phys. **A250** (1975) 163

13) I. R. Paschoupoulos, D. Phil. thesis, Oxford University (1975), unpublished
14) R. N. Glover and A. D. W. Jones, Nucl. Phys. **A84** (1966) 673
15) P. J. Brussaard and P. W. M. Glaudemans, Shell model applications in nuclear spectroscopy (North-Holland, Amsterdam, 1977) ch. 15
16) M. B. Johnson, L. W. Owen and G. R. Satchler, Phys. Rev. **142** (1966) 142
17) C. Gaarde and T. Kammuri, Nucl. Phys. **A215** (1973) 314
18) W. T. Pinkston and G. R. Satchler, Nucl. Phys. **A72** (1965) 641
19) S. Cohen and D. Kurath, Nucl. Phys. **A73** (1965) 1
20) W. Chung, D. Phil. thesis, Michigan State University (1976), unpublished
21) G. Bertsch, J. Borysowich, A. McManus and W. G. Love, Nucl. Phys. **A284** (1977) 399
22) J. J. Wesolowski, E. H. Schawarcz, P. G. Roos and C. A. Ludemann, Phys. Rev. **1**[illegible] (1968) 878
23) W. R. Wharton, J. G. Cramer, D. H. Wilkinson, J. R. Calarco and K. G. Nair, Phys. Rev. Lett. **31** (1973) 54
24) C. Gaarde, T. Kammuri and F. Osterfeld, Nucl. Phys. **A222** (1974) 579
25) R. Schaeffer, Nucl. Phys. **A158** (1970) 321
26) G. Cianguru, R. L. McGrath and F. E. Cecil, Phys. Lett. **61** (1976) 25
27) S. M. Austin, The two-body force on nuclei, ed. S. M. Austin and G. M. Crawley (Plenum, New York, 1972)
28) W. D. M. Rae, D. Phil. thesis, Oxford University (1976), unpublished
29) D. H. Feng, T. Udagawa and T. Tamura, Nucl. Phys. **A274** (1976) 262
30) W. R. Coker, T. Udagawa and H. H. Wolter, Phys. Rev. **C17** (1973) 1154
31) B. A. Brown, private communication
32) N. Anyais-Weiss, J. C. Cornell, P. S. Fisher, P. N. Hudson, A. Menchaca-Rocha, D. J. Millener, A. D. Panagiotou, D. K. Scott, D. Strottman, D. M. Brink, B. Buck, P. J. Elhs and T. Engeland, Phys. Reports **C12** (1974)
33) T. Tamura, T. Udagawa and M. C. Mermaz, unpubhshed
34) T. Une, S. Tamaji and H. Yoshida, Prog. Theor. Phys. **35** (1966) 1010
35) M. E. Williams-Norton, F. Petrovich, K. W. Demper, G. M. Hudson, R. J. Puigh and F. Zeller, Nucl. Phys. **A275** (1975) 509;
M. E. William-Norton *et al.*, Nucl. Phys. **A313** (1979) 477